Published in final edited form as:
Neuroscience. 2009 March 31; 159(3): 1055–1069. doi:10.1016/j.neuroscience.2009.01.023.

Vascular amyloid alters astrocytic water and potassium channels in mouse models and humans with Alzheimer's disease

Donna M. Wilcock*, **Michael P. Vitek**, and **Carol A. Colton**
Duke University Medical Center, Division of Neurology, Durham, NC 27710, USA.

Abstract

The neurovascular unit (NVU) comprises cerebral blood vessels and surrounding astrocytes, neurons, perivascular microglia and pericytes. Astrocytes associated with the NVU are responsible for maintaining cerebral blood flow and ionic and osmotic balances in the brain. A significant proportion of individuals with Alzheimer's disease (AD) have vascular amyloid deposits (cerebral amyloid angiopathy, CAA) that contribute to the heterogeneous nature of the disease. To determine whether NVU astrocytes are affected by the accumulation of amyloid at cerebral blood vessels we examined astrocytic markers in four transgenic mouse models of amyloid deposition. These mouse models represent mild CAA, moderate CAA with disease progression to tau pathology and neuron loss, severe CAA and severe CAA with disease progression to tau pathology and neuron loss. We found that CAA and disease progression both resulted in distinct NVU astrocytic changes. CAA causes a loss of apparent GFAP-positive astrocytic end-feet and loss of water channels (aquaporin 4) localized to astrocytic end feet. The potassium channels Kir4.1-an inward rectifying potassium channel and BK – a calcium-sensitive large-conductance potassium channel were also lost. The anchoring protein, dystrophin 1, is common to these channels and was reduced in association with CAA. Disease progression was associated with a phenotypic switch in astrocytes indicated by a loss of GFAP-positive cells and a gain of S100β-positive cells. Aquaporin 4, Kir4.1 and dystrophin 1 were also reduced in autopsied brain tissue from individuals with AD that also display moderate and severe CAA. Together, these data suggest that damage to the neurovascular unit may be a factor in the pathogenesis of Alzheimer's disease.

Keywords

CAA; astrocytes; amyloid; potassium channels; aquaporin; cerebrovasculature; Alzheimer's disease

Introduction

Alzheimer's disease (AD) is a progressive, neurodegenerative disorder characterized by extracellular amyloid deposits, intracellular neurofibrillary tangles and neuronal loss. In addition there are accompanying pathologies that likely contribute to progression of the disease including neuroinflammation (Akiyama et al., 2000) and cerebrovascular involvement (Nicoll et al., 2004). Accumulation of amyloid (amyloid β (Aβ) peptide) in the cerebrovasculature is associated with cerebral amyloid angiopathy (CAA) and has been reported to be present in 78–98% of all autopsied Alzheimer's cases with approximately 25–30% of these cases rated as severe CAA (Kalaria and Ballard, 1999).

*To whom correspondence should be addressed: Duke University Medical Center, Division of Neurology, Bryan Research Bldg, Box 2900, Research Dr, Durham, NC 27710, USA. E-mail: E-mail: donna.wilcock@duke.edu.
Section editor: Dr. Werner Sieghart

The blood –brain interface has been described as a functional unit commonly called the neurovascular unit (NVU) and is composed of cerebral blood vessels and closely juxtaposed cells including pericytes, perivascular microglia, perivascular neurons and astrocytes (Abbott, 2002;Iadecola, 2004). A primary function of this specialized region of the brain is to regulate the ionic composition of the extracellular milieu by altering local cerebral blood flow and transport across the blood-brain barrier. The NVU is well suited for this role since astrocyte end-feet impinge on the basement membrane of the blood vessel and are highly enriched with potassium channels and water channels (Abbott et al., 2006). One critical function of perivascular astrocytes is “potassium siphoning”, also known as potassium spatial buffering. This is a process whereby a local increase in extracellular K^+ ions produced by actively firing neurons results in influx of K^+ ions into the nearby astrocytes and a corresponding K^+ efflux from these astrocytes via the channels located on end feet near the blood vessels (Newman et al., 1984;Newman, 1986). Water movement via the aquaporin-4 water channel localized to astrocyte end-feet maintains osmotic balance and promotes effective K^+ siphoning (Nagelhus et al., 1999). Dysregulation of these processes has been shown in models of ischemia (Frydenlund et al., 2006), brain tumors (Warth et al., 2005) and epilepsy (Eid et al., 2005).

To study the effects of amyloid accumulation at cerebral vessels on the NVU, we utilized unique mouse models of Alzheimer’s disease that show all three primary pathological features of AD, that is, amyloid deposition, tau pathology and neuronal loss. These mice were created by crossing mouse strains expressing mutated human APP (APPSw or APPSwDI transgenic strains) with mice lacking the gene for inducible nitric oxide synthase (NOS2). In both the APPSw (Hsiao et al., 1996) and the APPSwDI mice (Davis et al., 2004) that only show amyloid deposition, deletion of the NOS2 gene results in progression of amyloid deposition to development of endogenous mouse tau pathology, neuron loss and behavioral deficits (Colton et al., 2006, Wilcock et al., 2008). Because these mice also demonstrated clear differences in the levels of amyloid deposition at cerebral blood vessels at 12 months of age, we compared astrocyte characteristics in mice with mild CAA (APPSw), moderate CAA with disease progression to tau pathology and neuron loss (APPSw/$NOS2^{-/-}$), severe CAA (APPSwDI) and severe CAA with disease progression to tau pathology and neuron loss (APPSwDI/$NOS2^{-/-}$). In general, the experimental results could be split into two categories; changes related to predominantly CAA and changes related to disease progression only. High levels of CAA were associated with an apparent loss of GFAP-positive astrocytic end-feet and loss of astrocytic machinery for potassium homeostasis. Disease progression worsened these effects but also resulted in a phenotypic switch in astrocytes indicated by loss of GFAP-positive cells and gain of S100β-positive cells. We found the same pathological characteristics in human Alzheimer’s disease tissue as a function of increasing severity of CAA. Our data emphasize the potential importance of an intact astrocyte network at the NVU and suggest that AD patients with CAA also have neurovascular pathology that may contribute to their clinical symptoms.

Experimental procedures

Animals

APPSw (Tg2576) mice transgenic for human APP with the Swedish mutation were obtained from K. Hsiao-Ashe (Hsiao et al., 1996). These were crossed to $NOS2^{-/-}$ mice yielding APPSw/$NOS2^{-/-}$ mice as previously described (Colton et al., 2006b). APPSwDI mice were obtained from W. Van Nostrand (Davis et al., 2004). These were crossed to $NOS2^{-/-}$ mice yielding APPSwDI/$NOS2^{-/-}$ mice as previously described (Wilcock et al., 2008). Age matched littermate $NOS2^{-/-}$ mice and wildtype mice were produced through the breeding colonies and maintained at Duke University under approved animal protocols. General pathological features of mice are shown in Table 1. Tau pathology and neuron loss was confirmed to be present in

the APPSw/NOS2$^{-/-}$ and APPSwDI/NOS2$^{-/-}$ mice used in these studies using standard techniques as previously described (Colton et al, 2006b; Wilcock et al, 2008).

Tissue processing and histological methods

Mice (52–56wks) were injected with a lethal dose of ketamine and perfused intracardially with 25ml normal saline. Brains were rapidly removed and bisected in the mid-sagittal plane. One half was immersion fixed for 24 hours in 4% paraformaldehyde (APPSw n=6, APPSw/NOS2$^{-/-}$ n=6, wildtype (WT) n=12, NOS2$^{-/-}$ n=12, APPSwDI n=6 and APPSwDI/NOS2$^{-/-}$ n=6). One half was snap frozen in liquid nitrogen and stored at −80°C. The hemibrains fixed in 4% paraformaldehyde were incubated for 24h in 10, 20 and 30% sucrose sequentially for cryoprotection. 40μm frozen sections were collected from APPSw, APPSw/NOS2$^{-/-}$ and their wildtype and NOS2$^{-/-}$ controls. 25μm frozen sections were collected for APPSwDI, APPSwDI/NOS2$^{-/-}$ and their wildtype and NOS2$^{-/-}$ controls. For studies on the APPSw and APPSw/NOS2$^{-/-}$ mice and their controls, 6–7 equally spaced sections 640μm apart were used. For studies on the APPSwDI and APPSwDI/NOS2$^{-/-}$ mice and their appropriate controls 7–8 equally spaced sections 600μm apart were used. Immunohistochemistry was performed for Aβ (rabbit polyclonal, 1:3000, Biosource, Camarillo, CA), aquaporin 4 (rabbit polyclonal, 1:1000, Chemicon, Temecula, CA), GFAP (rat monoclonal, 1:3000, Invitrogen, Carlsbad, CA) and S100β (mouse monoclonal, 1:3000, BD Biosciences, San Jose, CA) as previously described (Wilcock et al., 2004).

Analysis of S100β and vascular amyloid load

Total Aβ and S100β immunostained tissue was analyzed using a method previously described in detail (Wilcock et al., 2006). Briefly, percent area occupied by total Aβ immunostain was calculated. Images from the frontal cortex, CA1, CA3, dentate gyrus, subiculum and thalamus were collected from each section. An average of 4–5 sections for each animal were analyzed. Anatomical landmarks were used to ensure that the same region was assessed for each section examined. Using the Image-Pro Plus software we identified the positive stain on 2–3 representative images and the segmentation file was saved. This file was then applied to all images to yield measurements of percent area occupied with positive stain. For quantification of vascular amyloid we used a method described previously (Wilcock et al., 2006). The pools of Aβ (parenchymal and vascular) are clearly distinguishable by staining patterns (See Fig. 1).

Stereological analysis

GFAP-positive astrocyte processes that appeared to be contacting a blood vessel, aquaporin-4-positive blood vessels and GFAP-positive astrocyte cell bodies were counted in the hippocampus and the frontal cortex (N=4 for each group) using the optical fractionator method of stereological counting (West et al., 1991) with commercially available stereological software (StereoInvestigator, MBF Bioscience, Williston, VT) as described previously (Wilcock et al., 2008). A single experimenter performed all counting to ensure the same criteria were applied throughout. The regions of interests (ROI) were defined using specific landmarks within the tissue to maintain consistency. Section thickness was measured regularly on all collected sections to estimate the mean section thickness for each animal after tissue processing and averaged 12.34μm ± 0.32μm for the 25μm sections and 17.94μm for the 40μm sections. To count astrocytic processes, we used defined criteria established by careful examination of all sections at low and high magnification using differential interference contrast (DIC). These criteria were 1; the GFAP positive process must have a morphologically distinct end-foot appearance, 2; there must be an apparent blood vessel, distinguished at 600× magnification and 3; the process must trace back to an intact cell body. The reason for the inclusion of criteria number 3 was that occasionally we would observe astrocytic processes that terminated abruptly. Since it was unclear whether this was a cleaved process or simply that the astrocyte

cell body resided on another section, we excluded such processes. These criteria likely indicate that we significantly underestimated the total numbers of astrocytic end-feet, however, these criteria were necessary to maintain uniformity across all samples. Examples of processes counted can be seen in figure 2, panels B, D and F.

Human tissue

Rapid autopsy human brain samples were obtained from the Kathleen Price Bryan Brain Bank under Duke IRB approval. For this study paraffin embedded 10μm tissue sections and frozen samples from medial temporal lobe (cortical) brain tissue were prepared from individuals with confirmed mild, moderate and severe CAA with AD with Braak and Braak stage IV-V as well as age matched non-diseased controls. No significant differences were noted between age or post-mortem interval (PMI). Characteristics of the patient population are shown in Table 2. Paraffin was removed from tissue sections by immersion in xylene, rehydrated and stained for aquaporin-4 using immunohistochemical methods described previously (Wilcock et al., 2004).

Quantitative real-time RT-PCR

Approximately 40mg frozen brain powder was used for RNA extraction using the PerfectPure RNA tissue kit (5 Prime Inc., Gaithersburg, MD). RNA concentrations were determined and cDNA produced using the cDNA archive kit (Applied Biosystems, Foster City, CA). Real-time PCR was performed using the TaqMan Gene Expression assay kit (Applied Biosystems, Foster City, CA) according to the manufacturer's instructions and as previously described (Colton et al., 2006a). All genes are normalized to 18S rRNA and are shown as fold change vs the wildtype controls. The following genes were analyzed: 18S (ID#Hs99999901_s1), AQP4 (mouse ID# Mm00802131_m1, human ID# Hs00242342_m1), GFAP (mouse ID# Mm00546086_m1, human ID# Hs00157674_m1), Kir4.1 (mouse ID# Mm00445028_m1, human ID# Hs00157674_m1), Kv1.6 (mouse ID# Mm0049662_s1, human ID# Hs00266903_s1), dystrophin 1 (mouse ID# Mm00802400_m1, human ID# Hs00189308_m1), TASK2 (mouse ID# Mm00498900_m1), BK (mouse ID# Mm00516078_m1), Cx43 (Gja1 mouse ID# Mm00439105_m1).

Western blotting

Protein was extracted from 4 brains for each genotype using 50mg pulverized brain powder and quantified using the BCA protein assay kit (Pierce Biotechnology Inc. Rockford, IL. Performed according to manufacturer's instructions). 12μg protein samples from each brain lysate were run on a denaturing 4–20% SDS-PAGE gel. The gel was then transferred onto a nitrocellulose membrane. The transferred membrane was blocked in 5% non-fat milk and incubated overnight at 4°C in either anti-aquaporin-4 (1:1000), anti-Kir4.1 antibody (1:1000), anti-BK antibody (1:500, Millipore, Billerica, MA), anti-Kv1.6 (1:500, Millipore, Billerica, MA), anti-connexin 43 (1:1000, Millipore, Billerica, MA) or anti-dystrophin 1 (1:250, Sigma, Saint Louis, MO) and incubated for one hour in HRP conjugated anti-rabbit (for aquaporin 4, Kir4.1, BK, Kv1.6 or connexin 43) or HRP conjugated anti-mouse (for dystrophin 1) secondary antibody (1:2000). The membranes were developed using the ECL advance western blotting detection kit (GE Healthcare, Buckinghamshire, UK). Autoradiography film was exposed to the blot and developed. The blots were stripped using Restore stripping buffer (Pierce Biotechnology Inc, Rockford, IL). Each blot was then reprobed using the above protocol for GAPDH (mouse anti-GAPDH, Advanced ImmunoChemical Inc, Long Beach CA. 1:1,000,000) to ensure accurate gel loading. Western blot images were captured using the Kodak Image Station 440 (Carestream Health Inc, Rochester, NY) and semi-quantitative densitometry analysis was performed using the Kodak Molecular Imaging software

(Carestream Health Inc, Rochester, NY). Individual densitometry values were normalized to the GAPDH densitometry value on the same blot.

Data analysis

All immunohistochemical area data were analyzed by one-way analysis of variance (ANOVA) and student's t-test using the jmp7 statistical analysis software (SAS, Cary, NC). To compare stereological data from APPSw, which was sectioned at 40μm, to APPSwDI and APPSwDI/NOS2$^{-/-}$, which were sectioned at 25μm, we calculated their percent change from the matching wildtypes. This percent change was then analyzed by one-way ANOVA and student's t-test. Quantitative RT-PCR data was initially analyzed by calculating the individual fold-change values compared to the mean wildtype cycle number. The fold-change values were then analyzed by one-way ANOVA and student's t-test. Western blot data were pooled and normalized to the wild types included on the individual blot to normalize for differences between blots. Percent of wildtype values were calculated and one-way ANOVA and student's t-test was performed.

Results

To evaluate and compare the specific contributions of CAA alone, disease progression alone and the mixed actions of CAA and disease progression on the observed changes in astrocytes characteristics, we have associated each of the transgenic strains with a level of CAA and with the presence or absence of disease progression. For analysis of the effects of CAA alone, we have compared the APPSw (low CAA levels) to APPSwDI (high CAA levels). These mice strains do not show disease progression. The APPSwDI/NOS2$^{-/-}$ mice that show disease progression have equivalent amyloid levels and cerebrovascular distribution to the APPSwDI mice that show no disease progression. Comparing these strains allows us to evaluate the separate effects of disease progression on NVU changes. The APPSw/NOS2$^{-/-}$ has been examined separately since this mouse model has moderate CAA with disease progression. Consequently, changes associated with both CAA and disease progression are observed.

Cerebrovascular amyloid

In order to study the relationship between cerebrovascular amyloid deposition and astrocytic changes, we measured the levels of immunoreactive amyloid associated with blood vessels in the 4 mutant amyloid precursor protein (APP) mouse models used in this study. We found very low levels of vascular amyloid deposition in the APPSw (Tg2576) mice at 52 weeks of age (Fig. 1A). In age-matched APPSw/NOS2$^{-/-}$ mice, however, vascular amyloid staining was increased by 2 to 5 fold compared to the APPSw mouse alone (Fig.1B, C). The APPSwDI transgenic mice express the Dutch and Iowa mutations as well as the Swedish human APP mutations that direct amyloid deposition to the cerebrovasculature (Davis et al., 2004). Importantly, although APP expression levels are low (Davis et al., 2004), these mutations in Aβ impair its transport out of the brain (Davis et al., 2006) resulting in an overall higher level of soluble and insoluble Aβ peptides in the APPSwDI mice when compared to the APPSw or the APPSw/NOS2$^{-/-}$ mice (Table 1). As a consequence, the APPSwDI and the APPSwDI/NOS2$^{-/-}$ mice demonstrated higher levels of CAA than APPSw or APPSw/NOS2$^{-/-}$ mice at the same age. No significant differences were observed in the proportion of amyloid that was associated with cerebral vessels between the APPSwDI (Fig. 1D and F) and the APPSwDI/NOS2$^{-/-}$ mice (Fig. 1E and F).

Changes in morphological characteristics of neurovascular unit astrocytes

Astrocytes are a critical component of the NVU and serve as a link between neuronal activity and blood flow via the function of the astrocyte end-feet (Gordon et al., 2007;Takano et al., 2006;Mulligan and MacVicar, 2004;Wallraff et al., 2004). In the APPSw mice that

demonstrated low levels of cerebrovascular amyloid and no disease progression, we routinely observed direct contact between astrocyte end-feet and a morphologically distinct blood vessel (Fig. 2A). At high magnification (Fig. 2B) these end-feet and their associated astrocyte processes could be visually traced to an astrocyte cell body. A similar pattern of GFAP-positive staining was routinely observed in brain sections from wildtype and NOS2$^{-/-}$ control mice. In contrast, this normal morphology was altered in the APPSwDI mice where the number of astrocyte end-feet was less (Fig. 2C). At high magnification we observed an apparent lack of GFAP-positive end-feet that were clearly associated with a blood vessel (Fig. 2D). We observed a more dramatic loss of distinct astrocyte contact with the cerebrovasculature in the APPSwDI/NOS2−/− mice (Fig. 2E and F). We used unbiased stereology on serial sections to quantify the number of GFAP-positive astrocytic processes in contact with a morphologically distinct blood vessel that could be followed back to an identifiable astrocyte (GFAP+) cell body. We used defined criteria to define the processes that were counted (see materials and methods). We also counted the total number of GFAP-immunoreactive astrocyte cell bodies in the frontal cortex and hippocampus. A significant reduction in intact astrocyte end feet in direct contact with blood vessels was seen in the APPSwDI mice compared to NOS2$^{-/-}$ and APPSw mice (Fig. 2G, $P<0.01$). A further significant reduction was observed in the APPSwDI/NOS2$^{-/-}$ mice (Fig. 2G, $P<0.01$ compared to NOS2$^{-/-}$ and APPSwDI). Interestingly, total GFAP- immunopositive astrocyte cell number was significantly increased in the APPSw and the APPSwDI mice compared to wildtype and NOS2$^{-/-}$ mice (Fig. 2H, $P<0.01$) while this cell number was significantly decreased in the APPSwDI/NOS2$^{-/-}$ mice (Fig. 2H, $P<0.01$).

To determine whether the loss of GFAP-positive astrocytes in the APPSwDI/NOS2$^{-/-}$ mice indicated a true loss of astrocytes or a potential phenotypic switch from a passive to the complex subtype, we performed quantitative real-time RT-PCR and immunohistochemistry for S100β. Astrocytes are known to express GFAP, S100β or both and the expression profiles of these proteins relate to astrocyte function (Walz, 2000). S100β mRNA expression was significantly increased in APPSw and APPSwDI mice by 1.3–2 fold compared to wild-type or NOS2$^{-/-}$ control mice but was further increased by 5-fold in APPSwDI/NOS2$^{-/-}$ mice compared to controls (Fig. 3A). We also detected protein expression for S100β using immunohistochemistry. APPSw mice showed primarily cell body staining for S100β reminiscent of that observed in wildtype and NOS2$^{-/-}$ mice (Fig. 3B) while APPSwDI mice showed S100β staining in the cell bodies and also in occasional processes (Fig. 3C). However, in APPSwDI/NOS2$^{-/-}$ mice (Fig. 3D) S100β staining was significantly increased and was clearly seen in astrocytic processes. Quantification of S100β immunohistochemical staining by measuring percent area occupied with positive stain showed a significant increase in S100β staining in the frontal cortex and hippocampus of APPSw and APPSwDI mice compared to control mice (Fig. 3E). Again, there was a further significant increase in S100β staining in the APPSwDI/NOS2$^{-/-}$ mice (4-fold, Fig. 3E).

Passive astrocytes are extensively coupled via gap junctions, many of which include connexin 43 as a primary gap junction protein (Wallraff et al., 2004). To further examine a potential change in the number of passive and complex astrocytes, we used quantitative RT-PCR and Western blot to measure mRNA and protein levels, respectively, for connexin 43. APPSw mice showed a significant increase in connexin 43 mRNA compared to wild-type control mice. In contrast, connexin 43 mRNA was significantly decreased in both the APPSwDI and APPSwDI/NOS2$^{-/-}$ mice compared to either control mice or APPSw mice (Fig. 3F). Western blot analysis confirmed that protein levels for connexin 43 changed in a similar fashion as the mRNA in the APPSwDI and APPSwDI/NOS2$^{-/-}$ mice (Fig. 3G). Densitometry analysis normalized to GAPDH expression showed a significant, 50% decrease in band density in the APPSwDI mice while there was a further reduction of 60% in the APPSwDI/NOS2$^{-/-}$ mice when compared to wildtype or NOS2$^{-/-}$ (Fig. 3H).

Aquaporin 4 expression and localization

Aquaporin-4 (AQP4) is a bi-directional water channel with restricted localization to the astrocytic end-foot at the NVU in the brain (Badaut et al., 2002). In wild-type mice, the immunostaining for aquaporin 4 was localized primarily to the cerebrovasculature throughout the brain. As shown in Fig 4A for the CA3 region of the hippocampus, APPSw mice showed a comparable staining pattern to that of the wild-type and NOS2$^{-/-}$ mice. However, a decrease in aquaporin-4-positive blood vessels was observed in the frontal cortex or hippocampus of the APPSwDI (CA3 region, Fig. 4B) and a further decrease was seen in the APPSwDI/NOS2$^{-/-}$ (CA3 region, Fig. 4C). Using unbiased stereology to quantify the number of aquaporin-4 stained structures in the frontal cortex and hippocampus, we found a significant decrease in the number of aquaporin 4 positive blood vessels in APPSwDI mice (Fig. 4D, $P<0.05$ HPC and $P<0.01$ CX) compared with wild-type and NOS2$^{-/-}$ mice. APPSwDI/NOS2$^{-/-}$ mice had a further significant reduction ($P<0.01$ HPC and CX) in aquaporin 4 positive blood vessels.

We used quantitative RT-PCR to measure differences in mRNA expression of aquaporin 4 (Fig. 4E) and Western blot to determine protein expression (Fig. 4F) for AQP4. No significant differences were observed between any groups in either mRNA or protein expression levels.

Potassium channel expression

In addition to water channels, multiple subtypes of potassium channels are also localized to the membrane of astrocyte end feet. To determine if CAA and/or disease progression also affected potassium channels, we examined the mRNA and protein expression of Kir4.1, an inward rectifying voltage gated potassium channel and the BK channel; a calcium sensitive, large conductance potassium channel (Kofuji and Newman, 2004) (Price et al., 2002). We also measured mRNA and protein expression of the TASK2 channel which is a tandem-pore-domain potassium channel that is sensitive to changes in extracellular pH and is found in astrocytes (Rusznak et al., 2004). Expression of Kv1.6, a delayed rectifier voltage-gated potassium channel with widespread neuronal and glial distribution was used as a non-specific control (Smart et al., 1997). As shown in Fig. 5, mRNA levels of Kir4.1 and BK channels in APPSw mice were not significantly different from wild-type or NOS2$^{-/-}$ control mice. However, Kir4.1 and BK gene expression (Fig. 5A and B) was significantly reduced in APPSwDI and APPSwDI/NOS2$^{-/-}$ mice. The greatest levels of change in mRNA expression were observed for the Kir4.1 channel (60% reduction for APPSwDI mice and 70% reduction for APPSwDI/NOS2$^{-/-}$) with a 15% and 25% reduction for the BK channel in APPSwDI and APPSwDI/NOS2$^{-/-}$ mice, respectively. In contrast, TASK 2 gene expression was significantly increased in the APPSwDI mice while it was significantly decreased in the APPSwDI/NOS2$^{-/-}$ mice (Fig. 5C). No change in mRNA expression was observed for the Kv1.6 potassium channel in any of the mice examined (Fig. 5D).

Kir4.1, BK and Kv1.6 protein expression was measured by Western blot and quantified using densitometry with GAPDH as a loading control. There are no commercial antibodies currently available for mouse TASK2 so therefore we were unable to measure the protein expression of this channel. To compare samples from 2 separate blots we calculated the percentage change from wildtype controls on each blot. Again, no change was observed for APPSw mice compared to controls. However, we found decreased Kir4.1 protein expression in the APPSwDI and APPSwDI/NOS2$^{-/-}$ mice compared to wild-type and NOS2$^{-/-}$ mice (Fig. 5E). APPSwDI mice showed a 45% reduction ($P<0.01$) in Kir4.1 channel expression while a 65% reduction compared to wildtype ($P<0.01$) was seen in APPSwDI/NOS2$^{-/-}$ mice. BK protein expression was decreased in the APPSwDI and APPSwDI/NOS2$^{-/-}$ mice compared to wildtype and NOS2$^{-/-}$ mice (Fig. 5F). We found a 10% reduction in BK expression in APPSwDI mice ($P<0.05$) and a 20% reduction in BK expression in APPSwDI/NOS2$^{-/-}$ mice

compared to wildtype mice ($P<0.01$). Finally, no significant differences were observed in the Kv1.6 channel expression levels between mice strains (Fig. 5G).

Measurement of the anchoring protein, dystrophin 1

Dystrophin 1 is member of the dystrophin associated protein complex that serves to connect the extracellular matrix to the cytoskeletal network. This complex has been associated with intracellular signaling and regulation of aquaporin and potassium channels (Neely et al., 2001;Connors et al., 2004;Amiry-Moghaddam et al., 2003a). Using quantitative RT-PCR to measure differences in dystrophin 1 mRNA, we showed that mRNA expression was significantly reduced in mice with vascular amyloid deposition. APPSwDI mice showed a small (15%) but significant reduction in dystrophin 1 expression (Fig. 6A) while APPSwDI/NOS2$^{-/-}$ mice showed a 30% reduction in dystrophin 1 mRNA expression (Fig. 6A). Western blot analysis of dystrophin 1 protein levels revealed similar reductions to the gene expression in the mice with vascular amyloid deposition (Fig. 6B). Densitometry analysis of the western blot was performed and normalized to GAPDH. APPSwDI mice showed a more modest but significant 20% reduction in dystrophin 1 protein expression (Fig. 6C) while APPSwDI/NOS2$^{-/-}$ mice showed a 35% reduction (Fig. 6C).

The APPSw/NOS2$^{-/-}$ mouse

As shown in figure 1, the APPSw/NOS2$^{-/-}$ has significantly more CAA than the APPSw but significantly less than the APPSwDI/NOS2$^{-/-}$ mice that express high levels of CAA. Thus, the APPSw/NOS2$^{-/-}$ mouse represents moderate CAA with disease progression to tau pathology and neuron loss (Table 1). In general, the pathological features of the NVU resembled those observed in the APPSwDI/NOS2$^{-/-}$ mice. As depicted in Fig 7A, similar morphological changes were seen in the astrocytes in APPSw/NOS2$^{-/-}$ mice including damaged processes that were not associated with a cell body and reduced contact of end feet with blood vessels. Aquaporin 4 positive blood vessels in the hippocampus were reduced (Fig. 7B) while S100β-positive immunostaining of astrocytes was increased in the APPSw/NOS2$^{-/-}$ mice (Fig. 7C). Quantitation of the levels of mRNA and protein values or the number of structures is shown in Fig 7D. Of particular note is the significant increase in S100β and the significant decrease in GFAP-positive cell number as well as the large reduction in TASK2 mRNA expression. These changes are not observed in APPSwDI that have higher CAA levels compared to the APPSw/NOS2$^{-/-}$ but do not demonstrate disease progression.

Measurement of NVU markers in human Alzheimer's disease tissue

To examine the aquaporin 4, Kir4.1 and Kv1.6 channels in human Alzheimer's disease we obtained tissue sections and frozen brain chips from human AD samples Braak & Braak staging IV–V that had been classified as mild, moderate or severe cerebral amyloid angiopathy (CAA) (tissue characteristics are described in Table 2). Quantitative RT-PCR was used to measure mRNA expression levels of GFAP, aquaporin-4, Kir4.1, Kv1.6 and dystrophin 1 from the same human brain tissue. Severe CAA was associated with a significant decrease in GFAP mRNA expression (Fig. 8A) and a significant loss of aquaporin-4 gene mRNA expression (Fig. 8A). Reduced levels of Kir4.1 and dystrophin mRNA expression were seen in AD with both moderate and severe CAA while Kv1.6 expression was unchanged in any of the samples we examined (Fig. 8A). Aquaporin-4 immunohistochemistry in non-diseased, age matched tissue showed specific staining clearly associated with blood vessels throughout the sections (Fig. 8B). No major changes could be seen in the staining of AD tissue with mild CAA (Fig. 8C), while AD tissue with moderate CAA showed a diffuse pattern of staining with poorly distinguishable blood vessels (Fig. 8D). AD tissue with severe CAA showed little aquaporin 4 staining of blood vessels or diffuse staining throughout the tissue (Fig. 8E).

Discussion

AD has significant vascular risk factors such as the presence of CAA and microhemorrhage as well as hypertension, diabetes and hypercholesterolemia (de la Torre, 2002;Kalaria and Ballard, 1999). The neurovascular unit (NVU) is responsible for coupling the cerebral blood flow to local neuronal activity as well as maintaining the ionic and osmotic balances of the surrounding neuronal environment. (Abbott et al., 2006;Iadecola, 2004). In the current study we identify astrocyte changes associated with the NVU in transgenic mouse models of amyloid deposition with and without disease progression to tau pathology and neuron loss. The mouse models represent low CAA (APPSw), moderate CAA with disease progression (APPSw/NOS2$^{-/-}$), high CAA (APPSwDI) and high CAA with disease progression (APPSwDI/NOS2$^{-/-}$). We found that alterations in astrocytes can be broadly separated into CAA-dependent changes and disease progression dependent changes. We also found similar changes in human AD brain.

Cerebral vessel deposition of Aβ (CAA) is the major vascular pathology in AD. Comparison of the APPSw (low CAA), APPSwDI (high CAA) and APPSwDI/NOS2$^{-/-}$ (high CAA with disease progression) mice has allowed us to determine astrocytic changes associated with CAA alone and astrocytic changes associated with the presence of disease progression alone.

Astrocyte changes resulting from increased CAA

In mice with high CAA compared to mice with very low CAA, our data show that the numbers of astrocytic processes in apparent contact with cerebral vasculature are reduced. Similar regressive changes in astrocytes have been shown in Binswanger's disease, a form of vascular dementia characterized by diffuse white matter lesions (Akiguchi et al., 1997). To further assess CAA-associated changes in astrocytes at the neurovascular unit, we examined the levels of aquaporin 4 water channel and several potassium channels known to be highly expressed on astrocyte end feet that abut blood vessels. Aquaporin-4 is a water channel highly polarized to the astrocytic end-feet (Yang et al., 1995). We have found that transgenic mice with high levels of CAA have significant reductions in aquaporin-4 positive staining associated with the blood vessels. Interestingly, the effect is specific to the distribution of aquaporin 4 protein, since no change in total protein expression or gene expression was observed. Under normal conditions astrocytic end-feet are highly enriched with the inward rectifying potassium channel, Kir4.1 (Higashi et al., 2001) and the BK calcium dependent potassium channel (Price et al., 2002). Quantitative RT-PCR for these potassium channels indicated a significant decrease in gene expression levels in both the APPSwDI and APPSwDI/NOS2$^{-/-}$ mice that expressed high levels of CAA compared to APPSw mice that expressed low levels of CAA. Western blot confirmed that these changes extended to the protein level. Because voltage gated, delayed rectifier Kv1.6 channel expression which is globally distributed on astrocytes (Smart et al, 1997) was not altered in any of the mouse strains, these data imply that astrocyte end feet may be preferentially damaged by CAA. However, our western blot and quantitative real-time RT-PCR analyses on potassium channel expression were performed on whole brain homogenates. Thus, it is not possible to detect changes in potassium channels that are specific to the cerebrovasculature without further immunocytochemistry.

A potential explanation for the loss of aquaporin 4, Kir4.1 and BK channels is that they share a common anchoring protein that is affected by vascular amyloid deposition. The Dp71 dystrophin protein has been shown to be expressed in the CNS where it is localized to neuronal postsynaptic densities and perivascular astrocytes (Jancsik and Hajos, 1999) and where it serves to connect extracellular matrix with the intracellular cytoskeleton. Dystrophin is associated with β-dystroglycan, which in turn, associates with syntrophins. Genetic deletion of α-syntrophin has resulted in mislocalization of aquaporin 4 (Neely et al., 2001) and decreased perivascular Kir4.1 channel expression (Amiry-Moghaddam et al., 2003b;Fort et al., 2008).

Dystrophin-null mice also show a mislocalization of aquaporin 4 (Vajda et al., 2002). The BK channel is found co-localized with aquaporin 4 at astrocytic end-feet (Price et al., 2002) and data from C. elegans suggest that the BK channel also associates with dystrophin 1 (Carre-Pierrat et al., 2006). We measured gene and protein expression levels of dystrophin 1 and found significant reductions in mice with CAA. Thus changes in dystrophin levels and function may, in part, explain the loss of aquaporin-4 from the astrocyte end feet as well as the reduction in levels of Kir4.1 and BK channels in mice that express high levels of CAA. It is possible, however, that the selective loss of astrocytic end-feet directly results in loss of these channels.

The reduction in aquaporin and potassium channels that is associated with cerebrovascular amyloid deposition may have serious consequences to the brain. Astrocytes are known to maintain extracellular potassium concentrations in the brain by a process termed potassium siphoning (Orkand et al., 1966). This is a process whereby functionally coupled glial cells transfer K+ ions from regions of high extracellular K+ to regions of low extracellular K+ (Kofuji and Newman, 2004). Potassium siphoning helps to minimize changes in resting membrane potentials caused by extracellular potassium accumulation as well as regulate blood flow to active brain regions by either vasodilation or vasoconstriction depending on the potassium concentration (Knot et al., 1996;Horiuchi et al., 2002). Genetic deletion of Kir4.1 from astrocytes has been shown to significantly impair potassium siphoning (Djukic et al., 2007). Potassium efflux via BK channels at the astrocytic end foot has been shown to result in vasodilation suggesting a critical function for this channel in maintenance of vascular tone (Filosa et al., 2006). Blood flow changes including hypoperfusion have been observed in Alzheimer's disease (Drake and Iadecola, 2007). Thus, it is reasonable to predict that changes in potassium channel function may alter potassium buffering and potassium signaling at the vasculature leading to further brain impairment. Similar loss or mislocalization of aquaporin 4 and of Kir4 channels has been observed in the ischemic brain (Frydenlund et al., 2006;Milner et al., 2008;Pannicke et al., 2004;Iandiev et al., 2006).

Astrocyte changes resulting from disease progression

While we found that disease progression did, in fact, exacerbate the changes observed relative to CAA we also found other astrocytic changes that were dependent on disease progression alone. Mice with disease progression to tau pathology and neuron loss also lost GFAP-positive cells. In addition, connexin 43 protein was decreased while S100β immunostaining was increased. These changes suggest that disease progression initiates a change in the general phenotype of astrocytes from a passive to a complex subtype. Passive astrocytes are GFAP and S100β positive, extensively coupled via gap junctions and take up potassium ions while complex astrocytes express low levels of GFAP, are S100β positive and are not extensively coupled (Walz, 2000). A shift in astrocyte phenotype after mild ischemia towards the passive, highly coupled phenotype has been recently reported by Wang et al (Wang et al, 2008). In contrast, our data support the idea that astrocytes in the APPSw/NOS2$^{-/-}$ and APPSwDI/NOS2$^{-/-}$ mice resemble a more complex phenotype with loss of intracellular gap junction communication. It is unclear at this time whether we have observed a change in expression patterns of individual cells, losing GFAP expression and gaining S100β expression or whether, in fact, S100β-positive, GFAP-negative cells are undergoing proliferation while GFAP-positive cells are decreasing in number.

Disease progression is also associated with decreased levels of the TASK2 channel which may further contribute to a disruption of normal astrocyte function at the neurovascular unit. TASK2 is a member of the tandem-pore potassium channel family that modulates potassium currents in response to pH changes in the environment (Rusznak et al., 2004). Low pH has been shown to decrease TASK channel conductance and alter membrane potentials in neurons and glia (Taverna et al, 2005; Stansfeld et al, 2008). Loss of these channels may, therefore, result in

altered responses to acidification commonly associated with ischemia or other forms of neuronal damage.

APPSw/NOS2$^{-/-}$ mice

The APPSw/NOS2$^{-/-}$ mice were analyzed separately because of their intermediate levels of CAA. Although not as severe as the APPSwDI/NOS2$^{-/-}$ mice that show high levels of CAA, CAA related changes in astrocytic end-feet contact, aquaporin 4, Kir4.1, BK and dystrophin 1 expression and loss of connexin 43 were similarly observed in the APPSw/NOS2$^{-/-}$ mice. Also, the APPSw/NOS2$^{-/-}$ strain demonstrated changes consistent with disease progression; that is, loss of GFAP-positive cells, gain of S100β staining and loss of TASK2 expression.

Human Alzheimer's disease

While the functional significance of the observed changes in astrocyte morphology, water and potassium channel levels and distribution and expression of S100β, GFAP and gap junction proteins initiated by the presence of CAA and/or disease progression is not known, our data from the mouse models are highly reminiscent of changes associated with varying levels of CAA in humans with AD. We found that gene expression of Kir4.1 and dystrophin was significantly reduced in human AD post-mortem brain diagnosed with moderate and severe CAA. Aquaporin 4 and GFAP were only reduced in patients diagnosed with severe CAA. Kv1.6 channel expression was unchanged in any of the AD tissue samples. Aquaporin-4 protein expression at the blood vessel was reduced in those samples with moderate and severe CAA. Since each of the brain samples came from patients with advanced AD (Braak stage 4–5), it is unlikely that cognitive changes or disease progression were dominant factors in the difference in NVU pathology between individuals. Rather, the level of CAA was a clear, identifiable difference between these individuals. Thus, CAA may significantly contribute to the observed NVU pathology and may directly alter neuronal excitability through changes in astrocytes channels and function. Indeed, the high prevalence of seizures in Alzheimer's disease patients indicates altered neuronal excitability (Mendez et al., 1994;Lozsadi and Larner, 2006) which could be explained by a dysfunctional spatial potassium buffering system.

Conclusions

Overall, our data point to a critical role for the NVU in Alzheimer's disease as has previously been hypothesized (Zlokovic, 2005;Iadecola, 2004). We have shown in both mouse models of CAA and in humans with AD and CAA that vascular amyloid deposition results in mislocalization of aquaporin 4 expression and changes in expression levels of specific potassium channels, both of which are critical components of physiological systems designed to maintain the brain's external milieu. Disease progression results in altered astrocytic phenotype as well as exacerbation of the CAA-dependent changes. These novel findings provide a new mechanism for Alzheimer's disease and a potential avenue for the development of new therapeutics.

Acknowledgements

This work was supported by NIH grants AG030942 (DMW), AG19780 (MPV), AG19740 (CAC). M.P. Vitek is a Principal and Founder of Cognosci, Inc. No financial conflict exists with this study. Human tissue was kindly provided by the Bryan ADRC from the Kathleen Price Bryan brain bank (NIA P30 AG028377).

Abbreviations

APP, Amyloid precursor protein; Aβ, amyloid β peptide; AD, Alzheimer's disease; AQP4, aquaporin 4; CAA, Cerebral amyloid angiopathy; Cx43, connexin 43; GFAP, glial fibrillary acidic protein; NOS2, Nitric oxide synthase 2; NVU, Neurovascular unit.

Reference List

Abbott NJ. Astrocyte-endothelial interactions and blood-brain barrier permeability. J Anat 2002;200:629–638. [PubMed: 12162730]

Abbott NJ, Ronnback L, Hansson E. Astrocyte-endothelial interactions at the blood-brain barrier. Nat Rev Neurosci 2006;7:41–53. [PubMed: 16371949]

Akiguchi I, Tomimoto H, Suenaga T, Wakita H, Budka H. Alterations in glia and axons in the brains of Binswanger's disease patients. Stroke 1997;28:1423–1429. [PubMed: 9227695]

Akiyama H, et al. Inflammation and Alzheimer's disease. Neurobiol Aging 2000;21:383–421. [PubMed: 10858586]

Amiry-Moghaddam M, Otsuka T, Hurn PD, Traystman RJ, Haug FM, Froehner SC, Adams ME, Neely JD, Agre P, Ottersen OP, Bhardwaj A. An alpha-syntrophin-dependent pool of AQP4 in astroglial end-feet confers bidirectional water flow between blood and brain. Proc Natl Acad Sci U S A 2003a; 100:2106–2111. [PubMed: 12578959]

Amiry-Moghaddam M, Williamson A, Palomba M, Eid T, de Lanerolle NC, Nagelhus EA, Adams ME, Froehner SC, Agre P, Ottersen OP. Delayed K+ clearance associated with aquaporin-4 mislocalization: phenotypic defects in brains of alpha-syntrophin-null mice. Proc Natl Acad Sci U S A 2003b; 100:13615–13620. [PubMed: 14597704]

Badaut J, Lasbennes F, Magistretti PJ, Regli L. Aquaporins in brain: distribution, physiology, and pathophysiology. J Cereb Blood Flow Metab 2002;22:367–378. [PubMed: 11919508]

Carre-Pierrat M, Grisoni K, Gieseler K, Mariol MC, Martin E, Jospin M, Allard B, Segalat L. The SLO-1 BK channel of Caenorhabditis elegans is critical for muscle function and is involved in dystrophin-dependent muscle dystrophy. J Mol Biol 2006;358:387–395. [PubMed: 16527307]

Colton CA, Mott RT, Sharpe H, Xu Q, Van Nostrand WE, Vitek MP. Expression profiles for macrophage alternative activation genes in AD and in mouse models of AD. J Neuroinflammation 2006a;3:27. [PubMed: 17005052]

Colton CA, Vitek MP, Wink DA, Xu Q, Cantillana V, Previti ML, Van Nostrand WE, Weinberg JB, Dawson H. NO synthase 2 (NOS2) deletion promotes multiple pathologies in a mouse model of Alzheimer's disease. Proc Natl Acad Sci U S A 2006;103:12867–12872. [PubMed: 16908860]

Connors NC, Adams ME, Froehner SC, Kofuji P. The potassium channel Kir4.1 associates with the dystrophin-glycoprotein complex via alpha-syntrophin in glia. J Biol Chem 2004;279:28387–28392. [PubMed: 15102837]

Davis J, Xu F, Deane R, Romanov G, Previti ML, Zeigler K, Zlokovic BV, Van Nostrand WE. Early-onset and robust cerebral microvascular accumulation of amyloid beta-protein in transgenic mice expressing low levels of a vasculotropic Dutch/Iowa mutant form of amyloid beta-protein precursor. J Biol Chem 2004;279:20296–20306. [PubMed: 14985348]

Davis J, Xu F, Miao J, Previti ML, Romanov G, Ziegler K, Van Nostrand WE. Deficient cerebral clearance of vasculotropic mutant Dutch/Iowa Double A beta in human A betaPP transgenic mice. Neurobiol Aging 2006;27:946–954. [PubMed: 16105708]

de la Torre JC. Alzheimer disease as a vascular disorder: nosological evidence. Stroke 2002;33:1152–1162. [PubMed: 11935076]

Deane R, Wu Z, Sagare A, Davis J, Du YS, Hamm K, Xu F, Parisi M, LaRue B, Hu HW, Spijkers P, Guo H, Song X, Lenting PJ, Van Nostrand WE, Zlokovic BV. LRP/amyloid beta-peptide interaction mediates differential brain efflux of Abeta isoforms. Neuron 2004a;43:333–344. [PubMed: 15294142]

Deane R, Wu Z, Zlokovic BV. RAGE (yin) versus LRP (yang) balance regulates alzheimer amyloid beta-peptide clearance through transport across the blood-brain barrier. Stroke 2004b;35:2628–2631. [PubMed: 15459432]

Djukic B, Casper KB, Philpot BD, Chin LS, McCarthy KD. Conditional knock-out of Kir4.1 leads to glial membrane depolarization, inhibition of potassium and glutamate uptake, and enhanced short-term synaptic potentiation. J Neurosci 2007;27:11354–11365. [PubMed: 17942730]

Drake CT, Iadecola C. The role of neuronal signaling in controlling cerebral blood flow. Brain Lang 2007;102:141–152. [PubMed: 17010421]

Eid T, Lee TS, Thomas MJ, miry-Moghaddam M, Bjornsen LP, Spencer DD, Agre P, Ottersen OP, de Lanerolle NC. Loss of perivascular aquaporin 4 may underlie deficient water and K+ homeostasis in the human epileptogenic hippocampus. Proc Natl Acad Sci U S A Lanerolle 2005;102:1193–1198.

Filosa JA, Bonev AD, Straub SV, Meredith AL, Wilkerson MK, Aldrich RW, Nelson MT. Local potassium signaling couples neuronal activity to vasodilation in the brain. Nat Neurosci 2006;9:1397–1403. [PubMed: 17013381]

Fort PE, Sene A, Pannicke T, Roux MJ, Forster V, Mornet D, Nudel U, Yaffe D, Reichenbach A, Sahel JA, Rendon A. Kir4.1 and AQP4 associate with Dp71- and utrophin-DAPs complexes in specific and defined microdomains of Muller retinal glial cell membrane. Glia 2008;56:597–610. [PubMed: 18286645]

Frydenlund DS, Bhardwaj A, Otsuka T, Mylonakou MN, Yasumura T, Davidson KG, Zeynalov E, Skare O, Laake P, Haug FM, Rash JE, Agre P, Ottersen OP, miry-Moghaddam M. Temporary loss of perivascular aquaporin-4 in neocortex after transient middle cerebral artery occlusion in mice. Proc Natl Acad Sci U S A 2006;103:13532–13536. [PubMed: 16938871]

Gordon GR, Mulligan SJ, MacVicar BA. Astrocyte control of the cerebrovasculature. Glia 2007;55:1214–1221. [PubMed: 17659528]

Higashi K, Fujita A, Inanobe A, Tanemoto M, Doi K, Kubo T, Kurachi Y. An inwardly rectifying K(+) channel, Kir4.1, expressed in astrocytes surrounds synapses and blood vessels in brain. Am J Physiol Cell Physiol 2001;281:C922–C931. [PubMed: 11502569]

Horiuchi T, Dietrich HH, Hongo K, Dacey RG Jr. Mechanism of extracellular K+-induced local and conducted responses in cerebral penetrating arterioles. Stroke 2002;33:2692–2699. [PubMed: 12411663]

Hsiao K, Chapman P, Nilsen S, Eckman C, Harigaya Y, Younkin S, Yang F, Cole G. Correlative memory deficits, Abeta elevation, and amyloid plaques in transgenic mice. Science 1996;274:99–102. [PubMed: 8810256]

Iadecola C. Neurovascular regulation in the normal brain and in Alzheimer's disease. Nat Rev Neurosci 2004;5:347–360. [PubMed: 15100718]

Iandiev I, Tenckhoff S, Pannicke T, Biedermann B, Hollborn M, Wiedemann P, Reichenbach A, Bringmann A. Differential regulation of Kir4.1 and Kir2.1 expression in the ischemic rat retina. Neurosci Lett 2006;396:97–101. [PubMed: 16330144]

Jancsik V, Hajos F. The demonstration of immunoreactive dystrophin and its developmental expression in perivascular astrocytes. Brain Res 1999;831:200–205. [PubMed: 10411999]

Kalaria RN, Ballard C. Overlap between pathology of Alzheimer disease and vascular dementia. Alzheimer Dis Assoc Disord 1999;13:S115–S123. [PubMed: 10609690]

Knot HJ, Zimmermann PA, Nelson MT. Extracellular K(+)-induced hyperpolarizations and dilatations of rat coronary and cerebral arteries involve inward rectifier K(+) channels. J Physiol 1996;492(Pt 2):419–430. [PubMed: 9019539]

Kofuji P, Newman EA. Potassium buffering in the central nervous system. Neuroscience 2004;129:1045–1056. [PubMed: 15561419]

Lozsadi DA, Larner AJ. Prevalence and causes of seizures at the time of diagnosis of probable Alzheimer's disease. Dement Geriatr Cogn Disord 2006;22:121–124. [PubMed: 16733353]

Mendez MF, Catanzaro P, Doss RC, ARguello R, Frey WH. Seizures in Alzheimer's disease: clinicopathologic study. J Geriatr Psychiatry Neurol 1994;7:230–233. [PubMed: 7826492]

Milner R, Hung S, Wang X, Spatz M, Del Zoppo GJ. The rapid decrease in astrocyte-associated dystroglycan expression by focal cerebral ischemia is protease-dependent. J Cereb Blood Flow Metab 2008;28:812–823. [PubMed: 18030304]

Mulligan SJ, MacVicar BA. Calcium transients in astrocyte endfeet cause cerebrovascular constrictions. Nature 2004;431:195–199. [PubMed: 15356633]

Nagelhus EA, Horio Y, Inanobe A, Fujita A, Haug FM, Nielsen S, Kurachi Y, Ottersen OP. Immunogold evidence suggests that coupling of K+ siphoning and water transport in rat retinal Muller cells is mediated by a coenrichment of Kir4.1 and AQP4 in specific membrane domains. Glia 1999;26:47–54. [PubMed: 10088671]

Neely JD, miry-Moghaddam M, Ottersen OP, Froehner SC, Agre P, Adams ME. Syntrophin-dependent expression and localization of Aquaporin-4 water channel protein. Proc Natl Acad Sci U S A 2001;98:14108–14113. [PubMed: 11717465]

Newman EA. High potassium conductance in astrocyte endfeet. Science 1986;233:453–454. [PubMed: 3726539]

Newman EA, Frambach DA, Odette LL. Control of extracellular potassium levels by retinal glial cell K + siphoning. Science 1984;225:1174–1175. [PubMed: 6474173]

Nicoll JA, Yamada M, Frackowiak J, Mazur-Kolecka B, Weller RO. Cerebral amyloid angiopathy plays a direct role in the pathogenesis of Alzheimer's disease Pro-CAA position statement. NeurobiolAging 2004;25:589–597.

Orkand RK, Nicholls JG, Kuffler SW. Effect of nerve impulses on the membrane potential of glial cells in the central nervous system of amphibia. J Neurophysiol 1966;29:788–806. [PubMed: 5966435]

Pannicke T, Iandiev I, Uckermann O, Biedermann B, Kutzera F, Wiedemann P, Wolburg H, Reichenbach A, Bringmann A. A potassium channel-linked mechanism of glial cell swelling in the postischemic retina. Mol Cell Neurosci 2004;26:493–502. [PubMed: 15276152]

Pfeifer LA, White LR, Ross GW, Petrovitch H, Launer LJ. Cerebral amyloid angiopathy and cognitive function: the HAAS autopsy study. Neurology 2002;58:1629–1634. [PubMed: 12058090]

Price DL, Ludwig JW, Mi H, Schwarz TL, Ellisman MH. Distribution of rSlo Ca2+-activated K+ channels in rat astrocyte perivascular endfeet. Brain Res 2002;956:183–193. [PubMed: 12445685]

Rusznak Z, Pocsai K, Kovacs I, Por A, Pal B, Biro T, Szucs G. Differential distribution of TASK-1, TASK-2 and TASK-3 immunoreactivities in the rat and human cerebellum. Cell Mol Life Sci 2004;61:1532–1542. [PubMed: 15197476]

Saadoun S, Papadopoulos MC, Krishna S. Water transport becomes uncoupled from K+ siphoning in brain contusion, bacterial meningitis, and brain tumours: immunohistochemical case review. J Clin Pathol 2003;56:972–975. [PubMed: 14645363]

Smart SL, Bosma MM, Tempel BL. Identification of the delayed rectifier potassium channel, Kv1.6, in cultured astrocytes. Glia 1997;20:127–134. [PubMed: 9179597]

Takano T, Tian GF, Peng W, Lou N, Libionka W, Han X, Nedergaard M. Astrocyte-mediated control of cerebral blood flow. Nat Neurosci 2006;9:260–267. [PubMed: 16388306]

Vajda Z, Pedersen M, Fuchtbauer EM, Wertz K, Stodkilde-Jorgensen H, Sulyok E, Doczi T, Neely JD, Agre P, Frokiaer J, Nielsen S. Delayed onset of brain edema and mislocalization of aquaporin-4 in dystrophin-null transgenic mice. Proc Natl Acad Sci U S A 2002;99:13131–13136. [PubMed: 12232046]

Wallraff A, Odermatt B, Willecke K, Steinhauser C. Distinct types of astroglial cells in the hippocampus differ in gap junction coupling. Glia 2004;48:36–43. [PubMed: 15326613]

Walz W. Controversy surrounding the existence of discrete functional classes of astrocytes in adult gray matter. Glia 2000;31:95–103. [PubMed: 10878596]

Warth A, Mittelbronn M, Wolburg H. Redistribution of the water channel protein aquaporin-4 and the K+ channel protein Kir4.1 differs in low- and high-grade human brain tumors. Acta Neuropathol 2005;109:418–426. [PubMed: 15723236]

West MJ, Slomianka L, Gundersen HJ. Unbiased stereological estimation of the total number of neurons in thesubdivisions of the rat hippocampus using the optical fractionator. Anat Rec 1991;231:482–497. [PubMed: 1793176]

Wilcock DM, Gordon MN, Morgan D. Quantification of cerebral amyloid angiopathy and parenchymal amyloid plaques with Congo red histochemical stain. Nat Protoc 2006;1:1591–1595. [PubMed: 17406451]

Wilcock DM, Lewis MR, Van Nostrand WE, Davis J, Previti ML, Gharkholonarehe N, Vitek MP, Colton CA. Progression of amyloid pathology to Alzheimer's disease pathology in an amyloid precursor protein transgenic mouse model by removal of nitric oxide synthase 2. J Neurosci 2008;28:1537–1545. [PubMed: 18272675]

Wilcock DM, Rojiani A, Rosenthal A, Levkowitz G, Subbarao S, Alamed J, Wilson D, Wilson N, Freeman MJ, Gordon MN, Morgan D. Passive amyloid immunotherapy clears amyloid and transiently activates microglia in a transgenic mouse model of amyloid deposition. J Neurosci 2004;24:6144–6151. [PubMed: 15240806]

Yang B, Ma T, Verkman AS. cDNA cloning, gene organization, and chromosomal localization of a human mercurial insensitive water channel. Evidence for distinct transcriptional units. J Biol Chem 1995;270:22907–22913. [PubMed: 7559426]

Zlokovic BV. Neurovascular mechanisms of Alzheimer's neurodegeneration. Trends Neurosci 2005;28:202–208. [PubMed: 15808355]

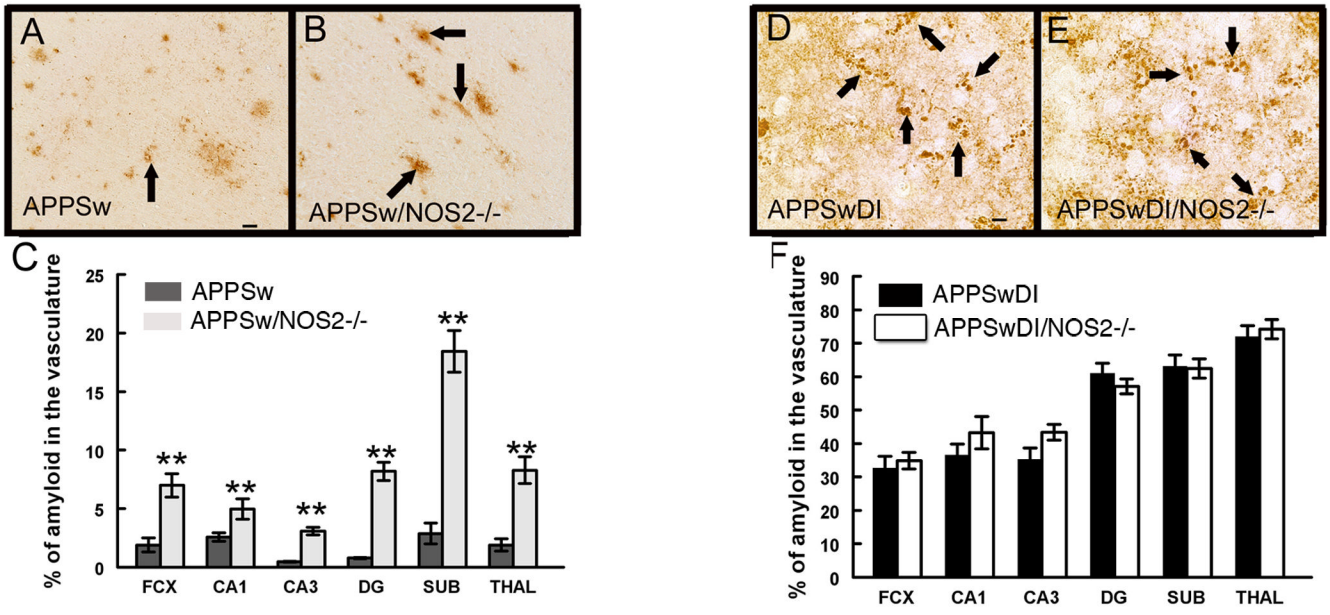

Figure 1.

Vascular amyloid deposition is increased when NOS2 is removed from APPSw mice, but not from APPSwDI mice. Panels A, B, D and E show Aβ immunohistochemistry at 52 weeks of age in APPSw (A), APPSw/NOS2$^{-/-}$ (B), APPSwDI (D) and APPSwDI/NOS2$^{-/-}$ (E) mice. 400× magnification. Scale bar A (for A and B) and C (for C and D): 6.25μm. Arrows indicate vascular amyloid. C and F shows quantification of vascular Aβ staining shown as an average percentage of total Aβ staining ± SEM. ** indicates P<0.01 compared to wildtype and NOS2$^{-/-}$ mice.

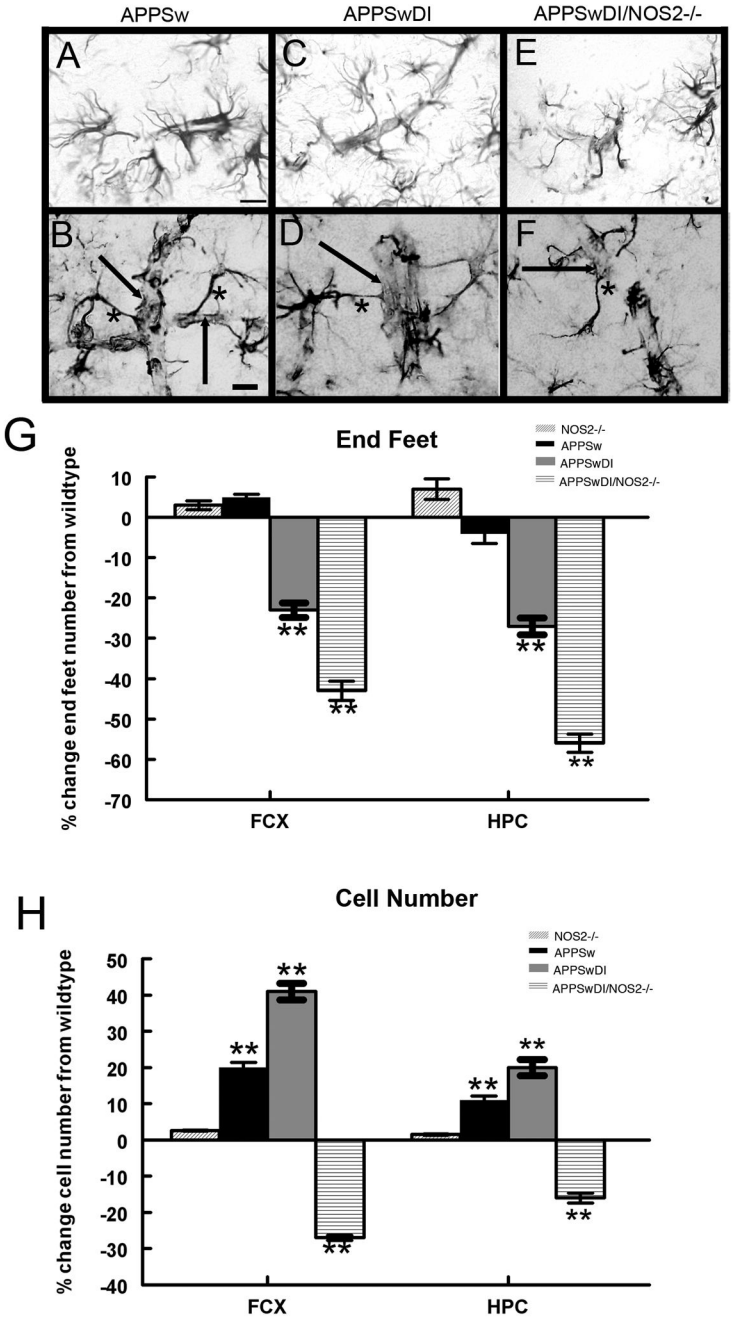

Figure 2.

GFAP positive astrocytes are reduced in APP mice when NOS2 is genetically deleted and their contact with blood vessels is significantly reduced in mice with high vascular amyloid. Panels A-F show GFAP immunohistochemistry of astrocytes surrounding blood vessels in APPSw (A and B), APPSwDI (C and D) and APPSwDI/NOS2$^{-/-}$ (E and F) mice. Panels A, C and E show 400× magnification, scale bar = 6.25μm. Panels B, D and F show 600× magnification using differential interference contrast (DIC), scale bar = 4.2μm. In panels B, D and F the arrows indicate a visible blood vessel wall while the asterisk shows an example of a GFAP-positive process that was counted. Panel G shows average results of stereological counts of intact astrocyte processes contacting blood vessels ± SEM. Panel H shows average

stereological quantification of astrocyte cell number ± SEM. ** indicates P<0.01 compared to wildtype and NOS2$^{-/-}$.

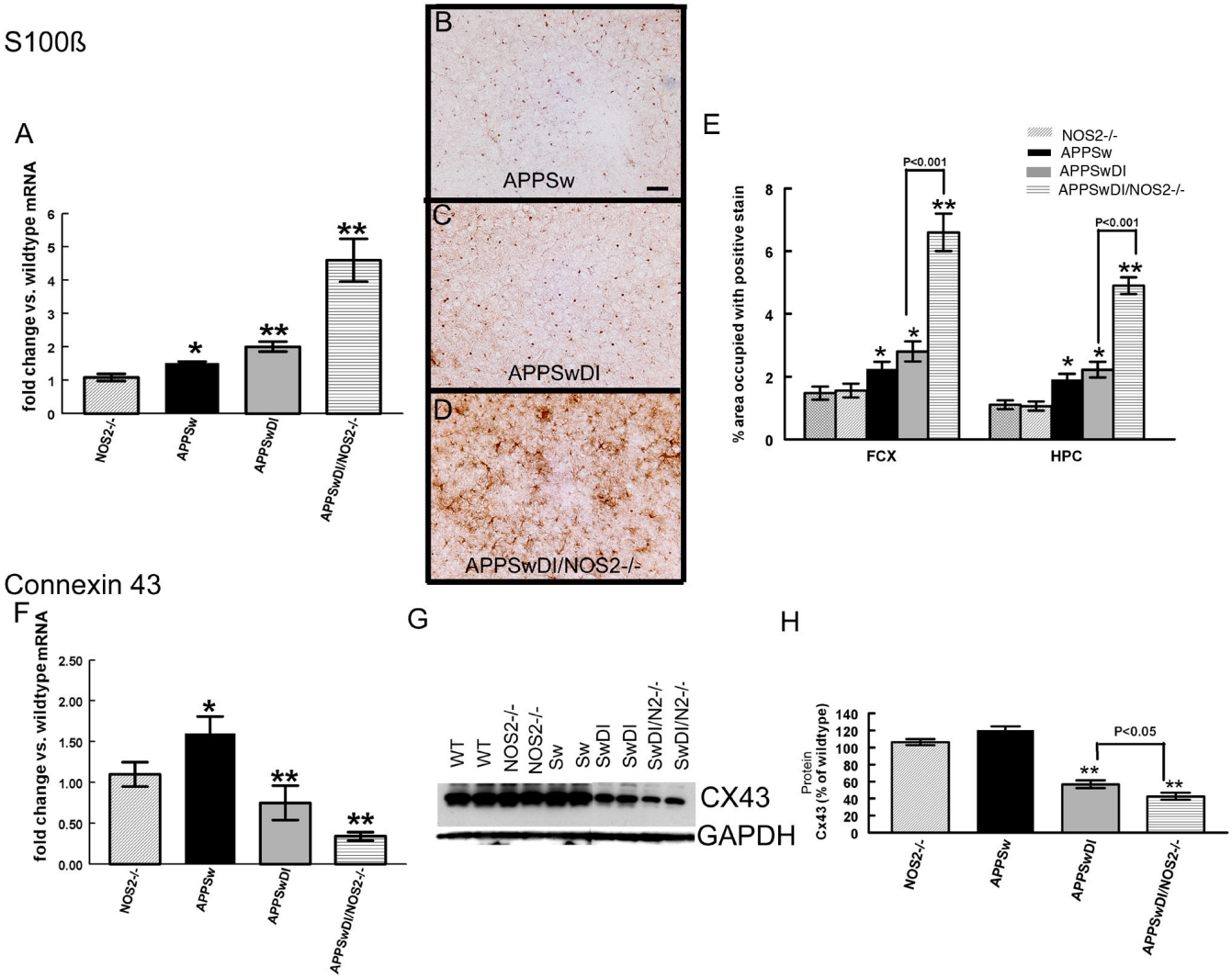

Figure 3.

Characteristics of astrocytes are changed in APP mice when NOS2 is genetically deleted. Panel A shows average quantitative real-time RT-PCR data for RNA expression levels of S100β ± SEM. Panels B-D show S100β S100β immunohistochemistry in frontal cortex of APPSw (B), APPSwDI (C) and APPSwDI/NOS2$^{-/-}$ (D) mice. 200× magnification, scale bar = 12.5μm. Panel E shows the average percent area occupied with positive stain for S100β in the frontal cortex and hippocampus ± SEM. Panel F shows average quantitative real-time RT-PCR data for connexin 43 RNA expression ± SEM. Panel G shows western blot for connexin 43 (CX43) and GAPDH in wildtype (WT), NOS2$^{-/-}$, APPSw (Sw), APPSwDI (SwDI), APPSwDI/NOS2$^{-/-}$ (SwDI/N2$^{-/-}$). Panel H shows average densitometry measurements of the western blot normalized to wildtype and shown as percent of wildtype± SEM. * indicates P<0.05, ** indicates P<0.01 compared to wildtype and NOS2$^{-/-}$ mice.

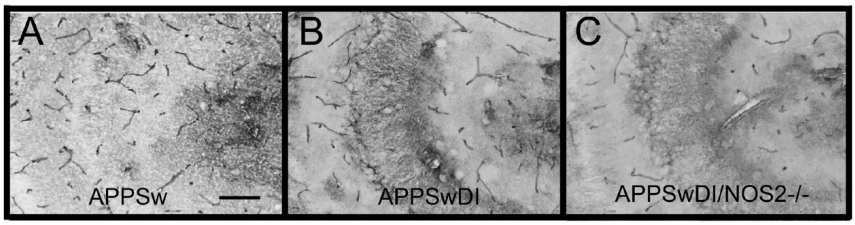

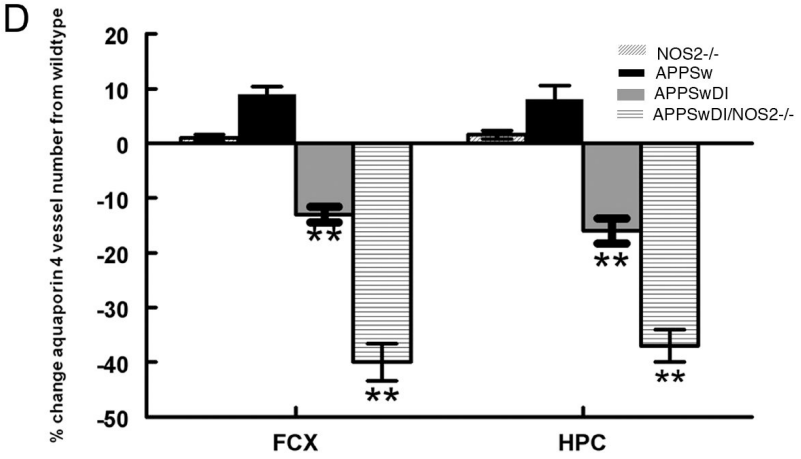

E

mRNA fold change	NOS2-/-	APPSw/ NOS2-/-	APPSwDI	APPSwDI/ NOS2--/-
Mean	1.12	1.23	1.15	1.3
SEM	0.03	0.18	0.15	0.08

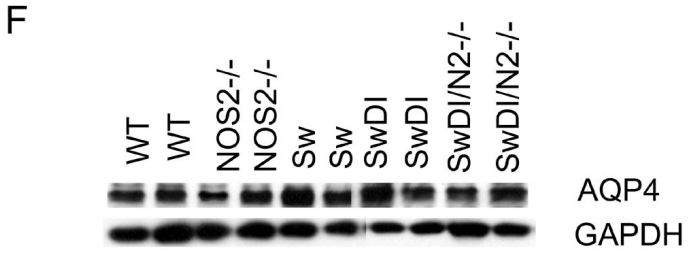

Figure 4.

Aquaporin-4 staining associated with blood vessels is reduced in mice with high vascular amyloid. Panels A – C show aquaporin-4 immunohistochemistry of blood vessels in the CA3 region of the hippocampus of APPSw (A), APPSwDI (B) and APPSwDI/NOS2$^{-/-}$ (C) mice. 200× magnification, scale bar = 12.5μm. Panel D shows the average number of vessels obtained from stereological counts of aquaporin-4 positive blood vessels ± SEM. ** indicates P<0.01 compared to wildtype and NOS2$^{-/-}$ mice. Panel E shows aquaporin 4 qRT-PCR data as the average fold change vs. wildtype ± SEM. Panel F shows representative western blot for aquaporin 4 and GAPDH for wildtype (WT), NOS2$^{-/-}$, APPSw (Sw), APPSwDI (SwDI), APPSwDI/NOS2$^{-/-}$ (SwDI/N2$^{-/-}$).

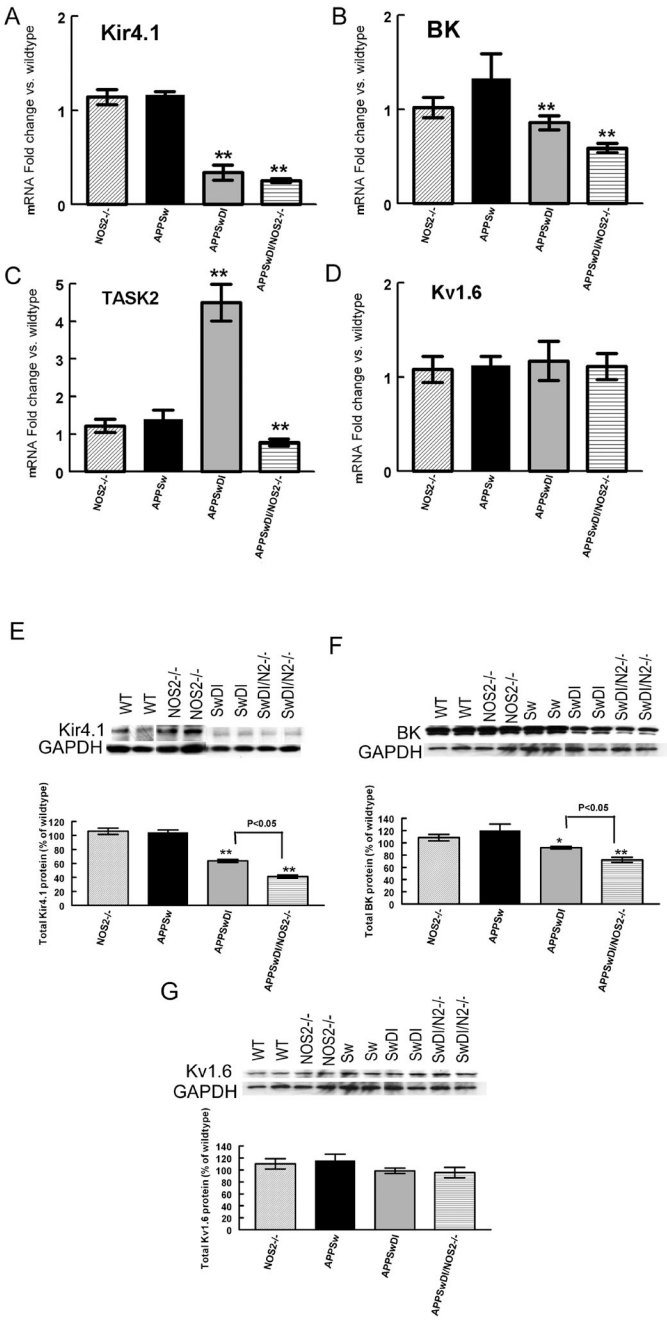

Figure 5.

mRNA expression levels of Kir4.1, BK and TASK2 are decreased in mice with vascular amyloid deposition. Panels A-D show average mRNA expression levels ± SEM for Kir4.1 (A), BK (B), TASK2 (C) and Kv1.6 (D) in $NOS2^{-/-}$, APPSw, APPSwDI and APPSwDI/$NOS2^{-/-}$ mice. All data are shown as fold change vs. wildtype. Panels E–G show representative western blots for Kir4.1 (E), BK (F) and Kv1.6 (G). For all blots the corresponding GAPDH blot is shown below. With the blots are graphs showing average densitometry data shown as percent change from wildtype ± SEM. On all blots: wildtype (WT), $NOS2^{-/-}$, APPSw (Sw), APPSw/$NOS2^{-/-}$ ($SwN2^{-/-}$), APPSwDI (SwDI), APPSwDI/$NOS2^{-/-}$ ($SwDI/N2^{-/-}$). ** indicates $P<0.01$ compared to wildtype and $NOS2^{-/-}$ mice.

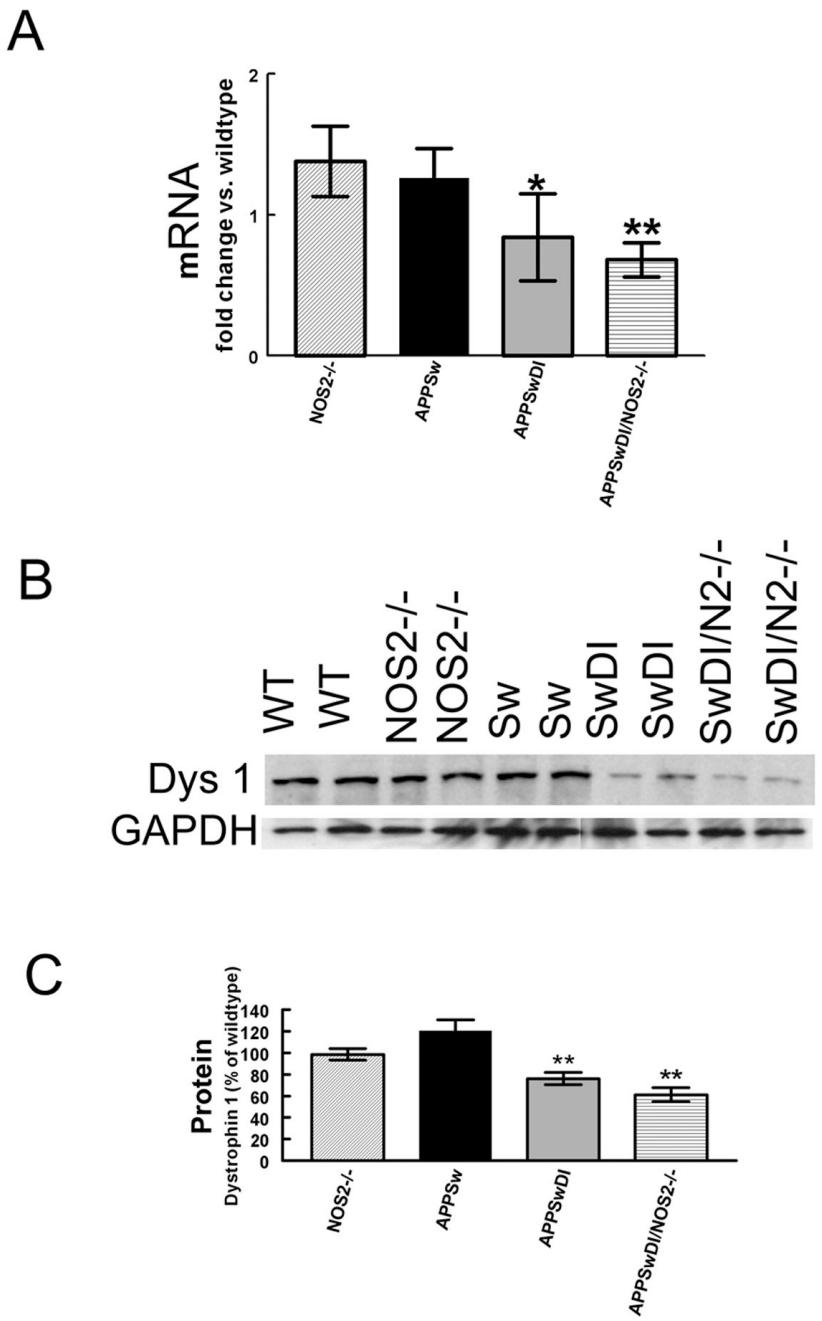

Figure 6.

Expression of the anchoring protein dystrophin 1 is reduced at both the RNA and protein level in mice with vascular amyloid deposition. Panel A shows quantitative real-time RT-PCR data for dystrophin-1. Data are expressed as the average fold change vs. wildtype ± SEM. Panel B shows a representative western blot for dystrophin 1 and corresponding GAPDH. On blot: wildtype (WT), NOS2$^{-/-}$, APPSw (Sw), APPSwDI (SwDI), APPSwDI/NOS2$^{-/-}$ (SwDI/N2$^{-/-}$). Graphs show densitometry data first normalized to GAPDH and then calculated as the average percent change from wildtype ± SEM. * indicates P<0.05, ** indicates P<0.01 compared to wildtype and NOS2$^{-/-}$ mice.

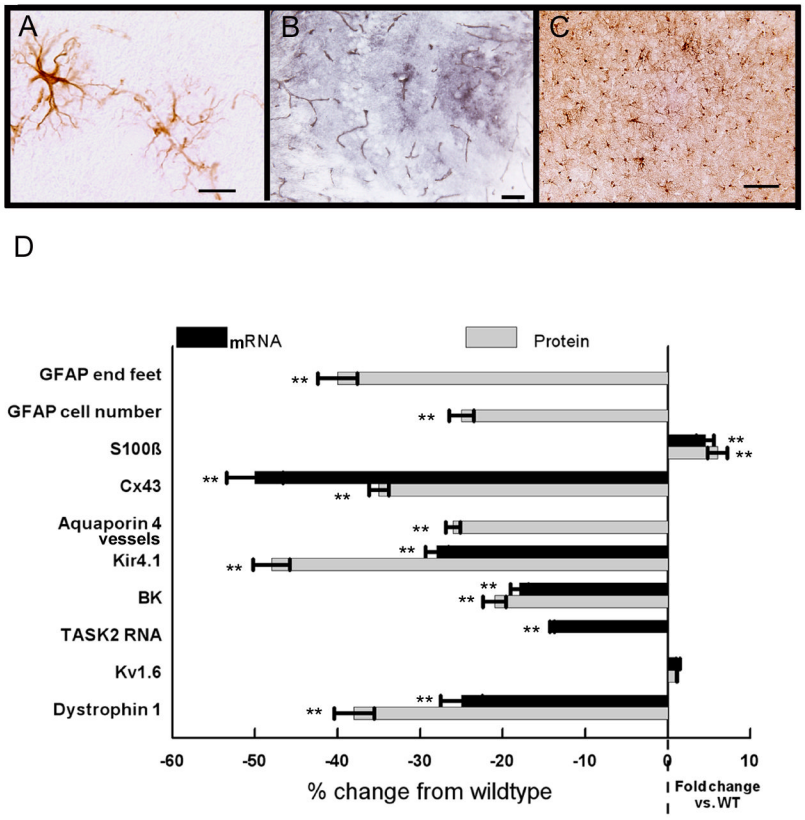

Figure 7.

APPSw/NOS2$^{-/-}$ mice show changes associated with both CAA and disease progression. Panels A-C show GFAP (A), aquaporin 4 (B) and S100β (C) staining for APPSw/NOS2$^{-/-}$ mice. A: frontal cortex, 600× magnification, scale bar = 4.2μm. B: CA3 and C: frontal cortex, 200× magnification, scale bar = 12.5μm. Panel D summarizes data for all markers examined using the same methods as described for other mice. Black bars: RNA, gray bars: protein. All data are shown as average fold change from wildtype ± SEM. ** indicates $P<0.01$ compared to wildtype and NOS2$^{-/-}$ mice.

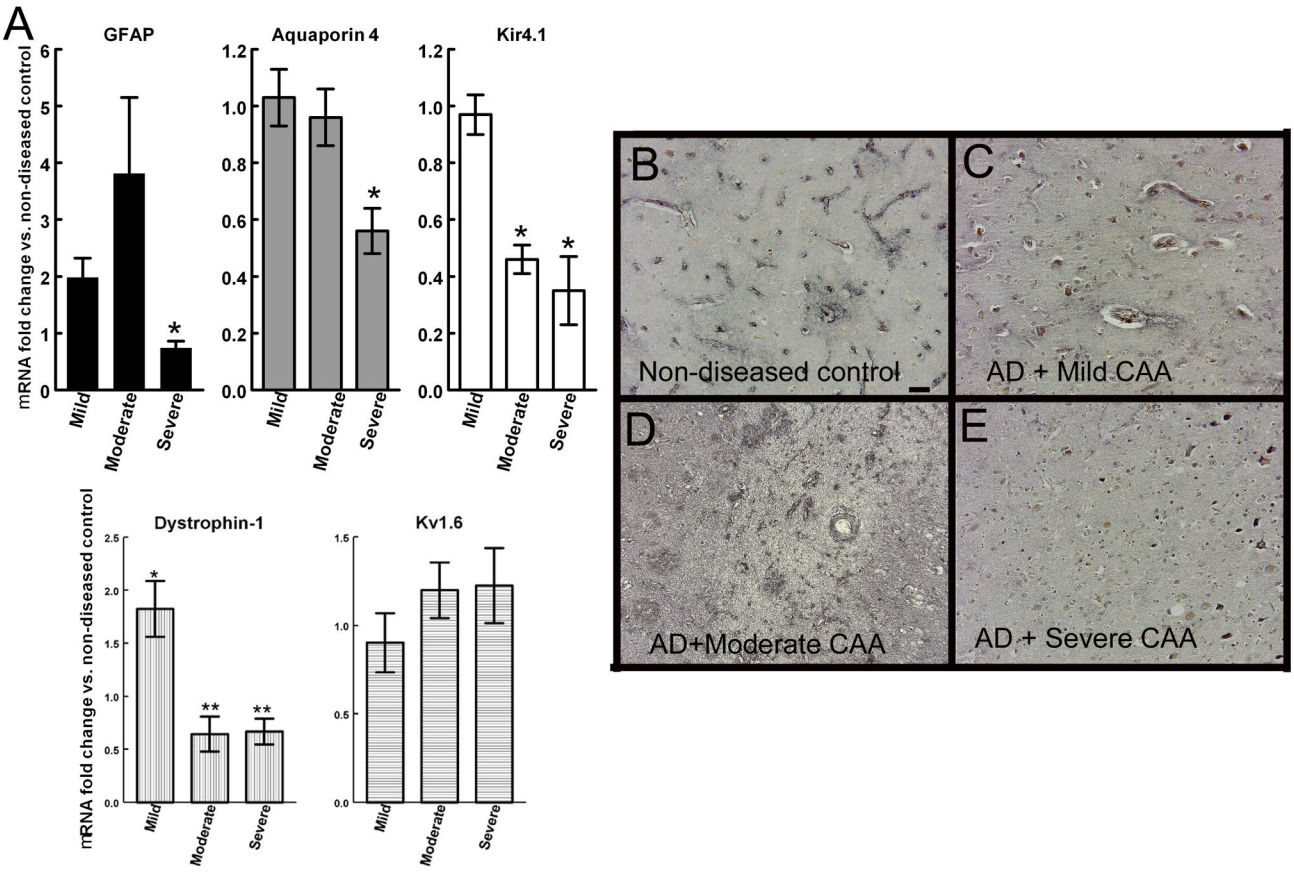

Figure 8.

Neurovascular unit disruptions are seen in Alzheimer's disease tissue. Panel A shows RNA expression levels of GFAP, aquaporin-4, Kir4.1, dystrophin 1 and Kv1.6 from AD tissue with mild, moderate and severe CAA. Data are shown as the average fold change vs. non-diseased control ± SEM. * indicates $P<0.05$, ** indicates $P<0.01$ compared to age-matched non-disease controls. Panels B–E show aquaporin-4 immunohistochemistry on human tissue sections from non-diseased brain (B), AD with mild CAA (C), AD with moderate CAA (D) and AD with severe CAA (E). 200× magnification, scale bar = 12.5μm.

TABLE 1

Comparison of AD pathologies in the transgenic mouse models used in these studies.

Mouse	APP transgene	Aβ levels (pg/ml)		Parenchymal amyloid	Vascular amyloid	Tau pathology	Neuron loss	Reference
		Soluble	Insoluble					
APPSw	Tg2576 – Swedish mutation	218±30	445±78	+	–	None	None	Hsiao et al. Science 274:99–102
APPSw/NOS2$^{-/-}$	Tg2576 – Swedish mutation	291±126	2881±960	+	+	++ AT8 and Thioflavin positive	30% HPC	Colton et al. Proc. Natl. Acad. Sci. USA 103:12867–12872
APPSwDI	Swedish, Dutch and Iowa mutations	1273±190	26321±5000	++	+++	None	None	Davis et al. J. Biol. Chem. 19:20296–20306.
APPSwDI/NOS2$^{-/-}$	Swedish, Dutch and Iowa mutations	1200±61	27544±4500	++	+++	++ AT8 and Thioflavin positive	30–40% HPC	Wilcock et al. J Neurosci 28:1537–1545.

+ indicates mild, ++ indicates moderate and +++ indicates severe.

TABLE 2

Characteristics of the human AD tissue examined.

Disease classification	Age	Sex	Braak & Braak score	PMI
AD +Mild CAA	80 ± 3.5	1 Male 2 Female	IV–V	14.5 hr ± 0.19
AD + Moderate CAA	81.67 ± 1.77	3 Female	IV–V	10 hr ± 0.13
AD + Severe CAA	82 ± 3	2 Male 1 Female	IV	13.5 hr ± 0.26
Normal controls	86.33 ± 0.88	3 Male 3 Female	I	12 hr ± 0.18